

## Comparison of Characteristics and Antimicrobial Activity of Synthesized Zinc Oxide And Magnetite Iron Oxide Nanoparticles Using Four Different Plant Extracts

Burcu Aydođdu <sup>1,a,\*</sup>, Mehmet Aytar <sup>2,b</sup>, İlky Ünal <sup>3,c</sup>

<sup>1</sup> Department of Mechanical Engineering, Faculty of Engineering, Munzur University, Tunceli, Türkiye.

<sup>2</sup> Department of Biology, Graduate School of Natural and Applied Sciences, Adnan Menderes University, Aydın, Türkiye.

<sup>3</sup> Department of Gastronomy and Culinary Arts, Faculty of Fine Arts, Design and Architecture Education, Munzur University, Tunceli, Türkiye.

\*Corresponding author

### Research Article

#### History

Received: 03/10/2023

Accepted: 12/01/2024




This article is licensed under a Creative Commons Attribution-NonCommercial 4.0 International License (CC BY-NC 4.0)


### ABSTRACT


The aim of this study was to synthesize Zinc oxide (ZnO) and magnetite iron oxide (Fe<sub>3</sub>O<sub>4</sub>) nanoparticles utilizing a precipitation method, employing plant extracts from *Ocimum basilica*(1), *Cinnamomum zeylanicum*(2), *Lactarius salmonicolor*(3) and *Paeonia kesrouanensis*(4) as reduction and stabilizing agents. Additionally, the antimicrobial activity of these nanoparticles against both gram-positive (*S. aureus*, ATCC 25923) and gram-negative (*E. coli*, ATCC 25922; *P. aeruginosa*, PAO1), bacteria as well as fungus (*C. albicans* 90028) was evaluated. The nanoparticles (NPs) were characterised by various analyses, including TEM, SEM, XRD, FTIR, DSL, and zeta potential. Based on the TEM image, the ZnONPs exhibited a cluster of flower-like structures, whereas the Fe<sub>3</sub>O<sub>4</sub>NPs displayed a spherical shape with a varying size distribution. The zeta potential values for ZnO NPs ranged from -5.35 to -16.9, while for Fe<sub>3</sub>O<sub>4</sub>NPs ranged from -7.43 to -20.7. All ZnO nanoparticles exhibited antimicrobial activity exclusively against the *S. aureus* strain, whereas Fe<sub>3</sub>O<sub>4</sub>NPs did not demonstrate any antibacterial effect.


**Keywords:** Antimicrobial activity, Green synthesis, Magnetite iron oxide, Zinc oxide

 [burcuaydogdu@munzur.edu.tr](mailto:burcuaydogdu@munzur.edu.tr)

 <https://orcid.org/0000-0002-3309-1995>

 [ilkayunal@munzur.edu.tr](mailto:ilkayunal@munzur.edu.tr)

 <https://orcid.org/0000-0002-1587-4187>

 [maytar90@gmail.com](mailto:maytar90@gmail.com)

 <https://orcid.org/0000-0002-8083-7358>

### Introduction

Nanoparticles (NPs) are particles in the nanoscale, typically ranging in size from 1 to 100 nanometers, and they exhibit distinctive characteristics and behaviours compared to their bulk counterparts, primarily because of their small size and high surface-to-volume ratio[1]. Overall, nanoparticles play an important role in advancing technology and have a wide range of applications in various industries including materials research, health, drug delivery, electronics, optics, environmental remediation, cosmetics, and sunscreens[2]. Their unique properties make them valuable building blocks for the development of innovative materials, devices and systems[3]. Zinc oxide nanoparticles are a widely used material in various applications such as electronics, antibacterial coatings, wound dressings and cosmetics due to their excellent high surface area to volume ratio, optical properties, semiconductor behavior, antibacterial and antifungal activity, photocatalytic activity, electrical conductivity and biocompatibility.[4]. Iron oxide nanoparticles, alternatively referred to as magnetic iron oxide nanoparticles or ferrite nanoparticles, have garnered substantial attention across multiple disciplines. superparamagnetism properties that make them valuable in a variety of applications like magnetic resonance imaging (MRI), drug delivery, and hyperthermia therapy[5]. Nanoparticles are typically synthesized using a

variety of techniques, including chemical, physical, and biological methods. Green synthesis refers to the production of nanoparticles using environmentally friendly and sustainable techniques using biomolecules, yeast, bacteria, plant or their extracts[6]. The green synthesis approach aims to minimize the use of hazardous chemicals and reduce the environmental impacts associated with conventional synthesis methods[7]. Plant extracts serve as natural sources of reducing and stabilizing agents. Other reasons for their use include the plant's easy availability, it's content of biocompatible bioactive compounds, and control of size and shape. It is important to note that the properties and characteristics of nanoparticles synthesized with plant extracts may vary depending on factors such as plant species, extract composition, synthesis conditions, and purification methods. *Aloe vera* and *neem* extracts have also been studied for the green synthesis of zinc oxide nanoparticles [8,9]. The choice of plant extract depends on factors such as availability, phytochemical composition, and desired nanoparticle properties[10]. Each plant extracts may contain additional bioactive components that impart specific properties to the synthesized nanoparticles. These components may include antioxidants, antimicrobial agents, anti-inflammatory compounds, and other bioactive molecules[11]. This offers the possibility

of imparting therapeutic or functional properties to nanoparticles, thus expanding their potential applications in biomedicine and healthcare. The type of plant used is important as the plant extract contains some proteins, enzymes and other phytochemicals that can act as different reducing and stabilizing agents during the synthesis of nanoparticles. *Ocimum basilicum* has been used to treat illnesses such as anxiety, fever, infections, arthropod stings, stomach aches, cough, headaches, and constipation [12]. The same time, Basil polysaccharides have anti-tumor, anti-oxidant, anti-bacterial effects as well as anti-aging activity, anti-atherosclerotic effects, immunity enhancing effect and are useful in the treatment of diabetes [13]. *Cinnamomum zeylanicum* was traditionally used to treat arthritis, diarrhea, allergies and ulcers [14]. *Paeonia kesrouanensis* is a plant frequently used in Chinese medicine and has been reported to have been used in various treatments for centuries [15]. When the antimicrobial activity of the plant against microorganisms was evaluated, it was seen that the extract of the plant was 3 times more effective than Vancomycin, Penicillin and Erythromycin and 2 times more effective than Tetracycline [16]. *Lactarius salmonicolor* has been found to have antitumor, antimicrobial, antiviral, antiallergic, immunomodulatory, anti-inflammatory, antiatherogenic, hypoglycemic, hepatoprotective and central nervous system activities [17].

The aim of this study is to realize the green synthesis of zinc and magnetite nanoparticles by using extracts of four different plants as reducing/stabilizing agents without using chemicals. In addition, the effects of the different plant extracts used on the morphological structures and antimicrobial activities of the 8 synthesized nanoparticles were comparatively evaluated. As a result, the usage area of nanoparticles can be determined according to their specific properties. Nanoparticles synthesized using four plant extracts were coded as ZnONPs-1 and Fe<sub>3</sub>O<sub>4</sub>NPs-1 (*Ocimum basilicum*), ZnONPs-2 and Fe<sub>3</sub>O<sub>4</sub>NPs-2 (*Cinnamomum zeylanicum*), ZnONPs-3 and Fe<sub>3</sub>O<sub>4</sub>NPs-3 (*Lactarius salmonicolor*), ZnONPs-4 and Fe<sub>3</sub>O<sub>4</sub>NPs-4 (*Paeonia kesrouanensis*). The ZnONPs and Fe<sub>3</sub>O<sub>4</sub>NPs were characterized by microscopic and spectroscopic methods. The antimicrobial activity was evaluated against *Staphylococcus aureus* (*S. aureus*, 25923), *Pseudomonas aeruginosa* (PAO1, *P. aeruginosa*), *Escherichia coli* (*E. coli* 25922), *Candida albicans* (*C. albicans* 90028) strains.

## Materials and Methods

### Reagents

Iron(II) chloride (FeCl<sub>2</sub>), Iron(III) chloride (FeCl<sub>3</sub>), Zinc acetate (Zn(CH<sub>3</sub>CO<sub>2</sub>)<sub>2</sub>·2H<sub>2</sub>O), Sodium hydroxide (NaOH), Potassium hydroxide (KOH) were purchased from Sigma-Aldrich. The plants were obtained from the local market.

### Preparation of the Plant Extract

*Ocimum basilicum*, *Cinnamomum zeylanicum*, *Lactarius salmonicolor*, *Paeonia kesrouanensis* were

washed several times to remove dirt and dried in the shade. 1 g of the plant was weighed and incubated individually in 100 mL of distilled water at 40°C for 24 hours. After cooling, it was filtered with filter paper and the filtrate was stored at 4°C.

### Preparation of Bio-synthesized ZnONPs and Fe<sub>3</sub>O<sub>4</sub>NPs

ZnONPs and Fe<sub>3</sub>O<sub>4</sub>NPs were synthesized using 4 different plant extracts. General synthesis procedure below:

**Synthesis of ZnONPs:** A 0.1 M 25 mL zinc acetate solution was prepared in a falcon tube and kept in a water bath at 50 °C for 1 hour. Then, 25 mL of plant extract was added. The pH was adjusted to 6 with KOH. The mixture was kept in a shaking water bath at 60 °C for 2 hours. After this time, the solution was centrifuged, washed and dried in an oven at 100 °C for 24 hours.

**Synthesis of Fe<sub>3</sub>O<sub>4</sub>NPs:** 50 mL 0.14 M FeCl<sub>2</sub> and 50 mL 0.17 M FeCl<sub>3</sub> solution were prepared in Falcon tubes and kept in a water bath at 70 °C for 1 hour. After reaching room temperature, the FeCl<sub>2</sub> and FeCl<sub>3</sub> solutions were mixed. The mixture was stirred for 1 hour. The pH was adjusted to 9 with NaOH. Then, 25 ml of plant extract was added. The mixture was again kept in a shaking water bath at 70 °C for 2 hours. After this time, the solution was centrifuged, washed and dried in an oven at 100 °C for 24 hours [18].

### Characterization Analysis

The crystallinity and structure of all samples were determined using X-ray diffractometer (XRD) Rigaku Miniflex (Japan) over a range of 2θ angles from 20° to 80°. Fourier transform infrared spectroscopy (FT-IR) was used to determine chemical functional groups of the samples using ATR-FTIR 6700 Jasco (Japan) in the 4000–400 cm<sup>-1</sup> range. The morphology of the nanoparticles were observed using transmission electron microscopy (TEM) (JOEL Brand, JEM-1011). Particle size and zeta potential value were measured using a Malvern Zetasizer Nano ZSP.

### Antimicrobial Activity

The agar well Diffusion method was used to test the antimicrobial activity of all ZnO NPs and Fe<sub>3</sub>O<sub>4</sub>NPs against gram-negative *Escherichia coli* (*E. coli*, ATCC 25922), *Pseudomonas aeruginosa* (*P. aeruginosa*, PAO1), gram-positive *Staphylococcus aureus* (*S. aureus*, ATCC 25923) and *Candida albicans* (*C. albicans* 90028) fungus. Gram-positive and gram-negative microorganisms were incubated overnight on Tryptic soy agar (TSA) at 37°C, while *C. albicans* fungus was set on Potato Dextrose Agar (PDA) at 28°C. After incubation, suspensions of microorganisms at 0.5 McFarland turbidity were prepared in physiological saline and standardized suspensions of each bacterium were placed on Mueller-Hinton agar plates. 8 mm diameter wells were punched in the petri using a sterile cork borer. 100 ml of each sample prepared at two different concentrations, 5 and 10 mg/mL, was

added to the wells. Gentamicin and fluconazole solutions were used as control antibiotics for bacteria and fungi, respectively. Antimicrobial activity was measured as a zone of inhibition (mm) around the sample discs using a standard steel ruler after 24 hours of incubation. The experiment was carried out in triplicate.

## Results and Discussion

### TEM Results

Shape and morphology of green synthesised ZnO NPs and Fe<sub>3</sub>O<sub>4</sub>NPs were evaluated by TEM analysis (Fig. 1).

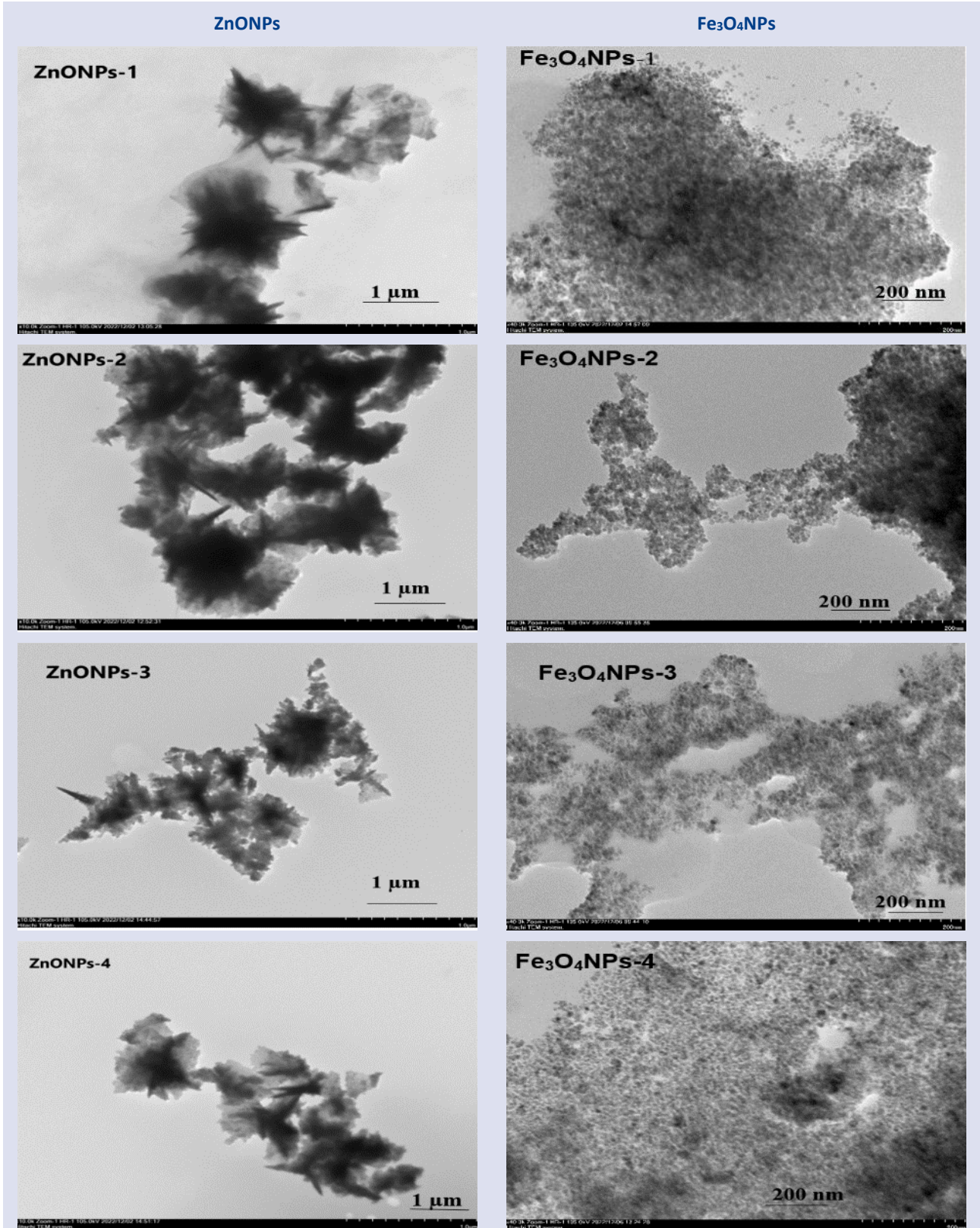


Figure 1. TEM image of ZnONPs and Fe<sub>3</sub>O<sub>4</sub>NPs



According to the TEM image, the ZnONPs showed a flower-like structure cluster, while the Fe<sub>3</sub>O<sub>4</sub>NPs had a spherical shape with different size distribution.

Among the synthesized NPs, ZnNPs-4 showed a smaller size distribution, while Fe<sub>3</sub>O<sub>4</sub>NPs-3 had a uniform and single-crystal. The size and shape of the NPs can be controlled according to experimental conditions, such as ratios of reactants, reducing/stabilizing agents, temperature, and time [19]. ZnONPs and Fe<sub>3</sub>O<sub>4</sub>NPs have different shapes such as rod-like, star-like, spiral, flower-like, cubes, triangles, or tetrapods, and isometric [20]. NP shapes are one of the most important factors influencing their areas of application. Mazitova et al. (2018) synthesized flower-like-ZnO nanoparticles by laser ablation of solid targets in a liquid [21].

**XRD Results**

The XRD results of synthesized ZnONPs and Fe<sub>3</sub>O<sub>4</sub> NPs are given in Figure 2. The XRD spectrum of all Fe<sub>3</sub>O<sub>4</sub>NPs samples showed an intense diffraction peak at the 2θ regions corresponding to the crystal planes by Miller index (111), (220), (400), (422), (511), (440), and (531). The XRD pattern also showed that the particles have a face-centred cubic (FCC) crystal structure[22]. In addition, The miller index corresponding to the 100 plane shows that znO is hexagonal. (100), (002), (101), (102), (110), (103), (200), (112), (201), (004), and (202) planes of hexagonal ZnO nanoparticles (JCPDS 36-1451)[23].

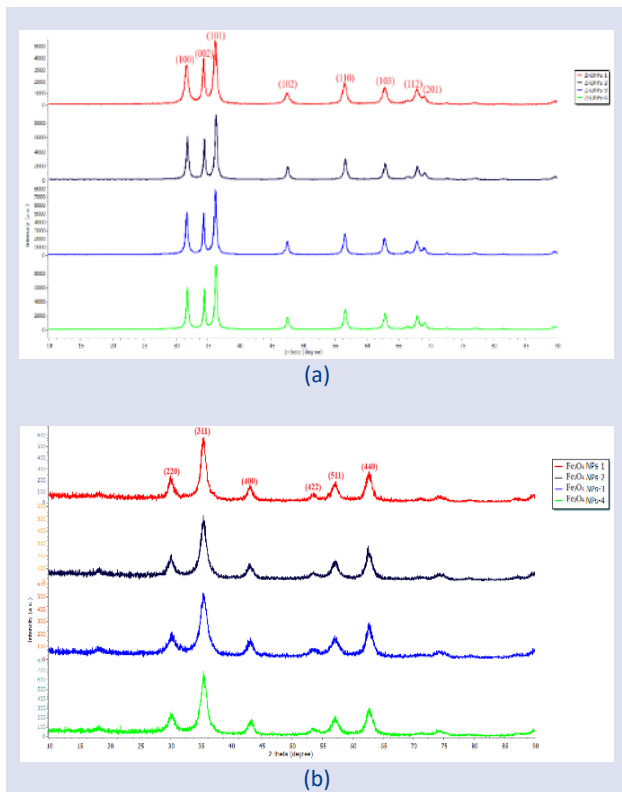


Figure 2. XRD graphs a) ZnONPs-1(red line), ZnONPs-2(navy blue line), ZnONPs-3 (blue line), ZnONPs-4 (green line) b)Fe<sub>3</sub>O<sub>4</sub>NP-1(red line), Fe<sub>3</sub>O<sub>4</sub>NP-2(navy blue line), Fe<sub>3</sub>O<sub>4</sub>NP-3 (blue line), Fe<sub>3</sub>O<sub>4</sub>NP-4 (green line)

ZnONPs exhibited more sharper and narrower XRD peaks, whereas Fe<sub>3</sub>O<sub>4</sub>NPs displayed broader peaks. This indicates that the phytochemicals present on the surface of the nanoparticles break the crystalline structure and make them amorphous. The average nanoparticle crystallite size was calculated from XRD peak broadening using the Debye-Scherrer equation for characteristic peaks.

$$D = K\lambda/\beta\cos\theta$$

where D represents the average diameter in nm, K presents the Scherrer constant (0.89), λ presents the wavelength of the X-ray (λ = 0.154056 nm), β presents the corresponding full width at half maximum (FWHM) of the peaks is the diffraction peak and θ represents the Bragg diffraction angle. The results are given in Tables 1-2. It was observed that the crystal size of Fe<sub>3</sub>O<sub>4</sub>NPs was lower than that of ZnONPs, which was compatible with the DLS results

Table 1. Average XRD crystallite size of the ZnONPs

Peak Number	Planes hkl	2θ			
		ZnONPs-1	ZnONPs-2	ZnONPs-3	ZnONPs-4
1	100	31.70	31.85	31.70	31.80
2	002	34.30	34.53	34.40	34.49
3	101	36.12	36.33	36.21	36.29
4	102	47.54	47.60	47.51	47.59
5	110	56.50	56.67	56.58	56.65
6	103	62.66	62.95	62.78	62.95
7	112	67.83	67.96	67.98	67.93
8	201	68.97	69.08	69.11	69.04
XRD Crystallite Size of The Samples		17.60 nm	20.11 nm	19.70 nm	21.52 nm

Table 2. Average XRD crystallite size of the Fe<sub>3</sub>O<sub>4</sub>NPs

Peak Number	Planes hkl	2θ			
		Fe <sub>3</sub> O <sub>4</sub> NPs-1	Fe <sub>3</sub> O <sub>4</sub> NPs-2	Fe <sub>3</sub> O <sub>4</sub> NPs-3	Fe <sub>3</sub> O <sub>4</sub> NPs-4
1	220	29.80	30.13	30.32	30.16
2	311	35.41	35.38	35.30	35.47
3	400	43.09	43.03	43.22	43.18
4	422	53.54	53.80	53.71	53.82
5	511	57.07	57.12	57.20	57.13
6	440	62.61	62.48	62.57	62.55
XRD Crystallite Size of The Samples		7.93 nm	6.45 nm	5.84 nm	6.24 nm

**FT-IR Results**

FTIR was used to analyze the presence of possible functional groups responsible for nanoparticle reduction and capping (Fig.3). Phytochemicals such as alcohols, phenols, amines, carboxylic acids, and others present in plant extracts have the capability to interact with the surfaces of zinc and iron, thereby aiding in the stabilization of nanoparticles. The broad peak within the 3400-3300 cm<sup>-1</sup> range, a common occurrence in FTIR spectra,

provides confirmation of the existence of intermolecular hydrogen bonding[24]. The absorption peaks at approximately  $\sim 1570$  and  $\sim 1400$   $\text{cm}^{-1}$  in both spectra, known to come from plant extracts and help particle synthesis, are assigned to C=C stretching and C-C stretching vibrations, respectively. The bands at approximately  $\sim 850$   $\text{cm}^{-1}$  and  $\sim 757$   $\text{cm}^{-1}$  are attributed to primary amine and N-H deformation bands. Metal-

oxygen bond exhibits distinctive absorption bands within the wavenumber range of 400 to 600  $\text{cm}^{-1}$  [25]. The absorption peaks around 535  $\text{cm}^{-1}$  observed in the spectra of  $\text{Fe}_3\text{O}_4$ NPs are attributed to Fe-O bending vibration[26][22]. Similarly, the peaks observed at approximately 600  $\text{cm}^{-1}$  in the FTIR spectra of ZnONPs correspond to Zn-O stretching[23], respectively.

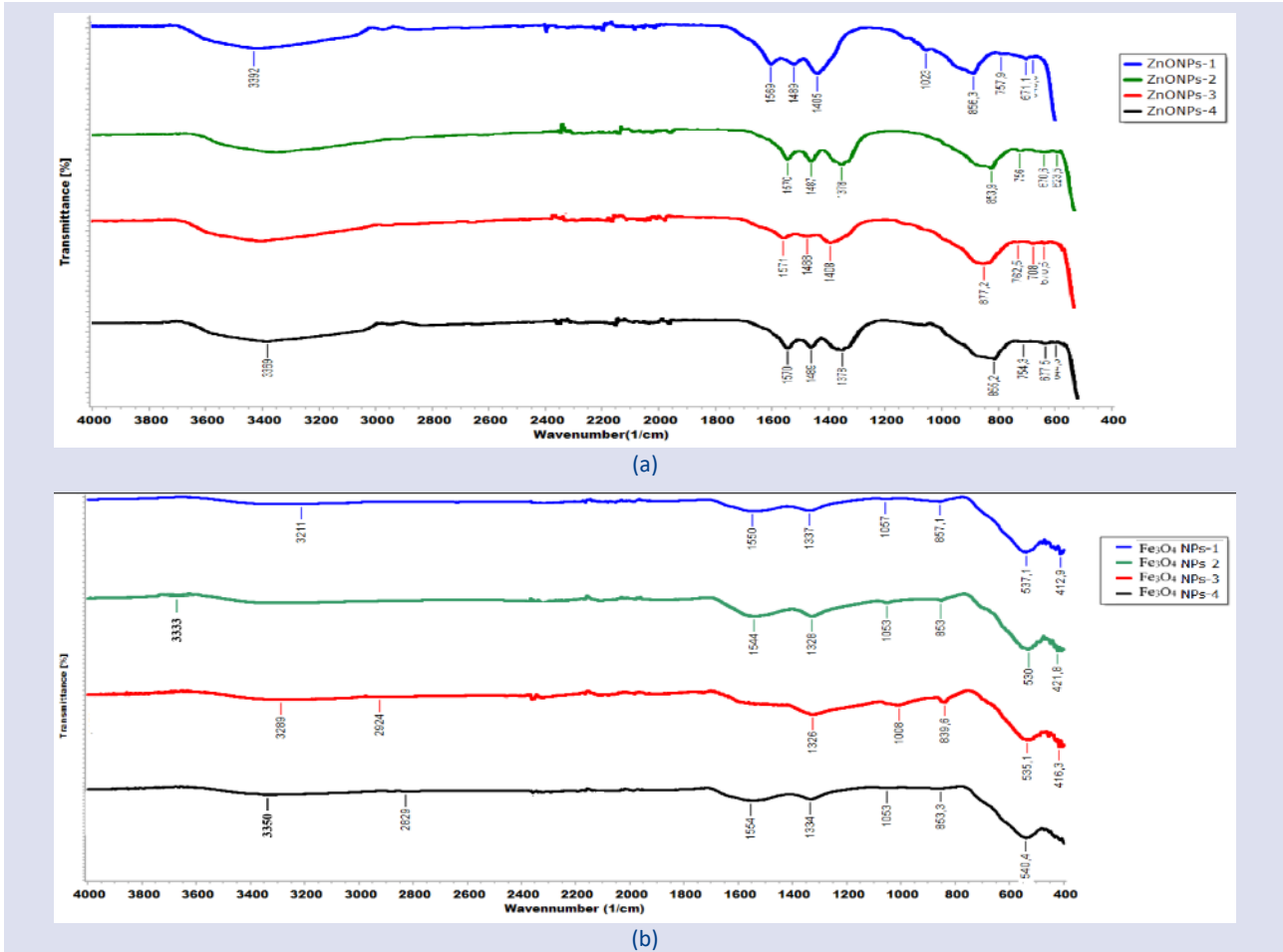


Figure 3. FTIR spectrum of a) ZnONPs-1(blue line), ZnONPs-2(green line), ZnONPs-3 (red line), ZnONPs-4 (black line) b) $\text{Fe}_3\text{O}_4$ NP-1((blue line),  $\text{Fe}_3\text{O}_4$ NP-2(green line),  $\text{Fe}_3\text{O}_4$ NP-3 (red line),  $\text{Fe}_3\text{O}_4$ NP-4 (black line)

**DLS and Zeta Potential Results**

Dynamic light scattering (DLS) is a widely used technique for determining particle size in colloidal suspensions.[27] The parameter used to define the size range in the particle size distribution is called the "polydispersity index" (PDI). This index indicates that values less than 0.05 are essentially highly monodisperse, while PDI values greater than 0.7 indicate that the sample has a very broad particle size distribution[28]. The zeta potential is a very important parameter that provides information about the stability of particles. As the zeta potential increases, particles are prevented from coming together and forming aggregates due to the greater electrostatic repulsion between them, increasing the stability of the colloidal suspension.[29]. The zeta potential is closely related to the morphology of the

particle surface. The particle size distributions, PDI value and zeta potentials of the zinc and iron NPs are shown In Figure 4 and Table 3. ZnONP-3 and ZnONP-4, which have a low PDI value, showed a more homogeneous distribution while all  $\text{Fe}_3\text{O}_4$ NPs with high PDI values showed a heterogeneous size distribution. All nanoparticles were found to have a high size distribution. Metal nanoparticles often tend to agglomerate by sticking together. This agglomeration process can result in larger differences in particle sizes. Nanoparticle agglomeration can occur during the drying process due to Van der Waals forces or chemical interactions[30]. The zeta potential values of the NPs differed according to the type of plant extract. While this value was between -5.35 and -16.9 for ZnONP's, it changed between -7.43 and -20.7 for  $\text{Fe}_3\text{O}_4$ NPs.

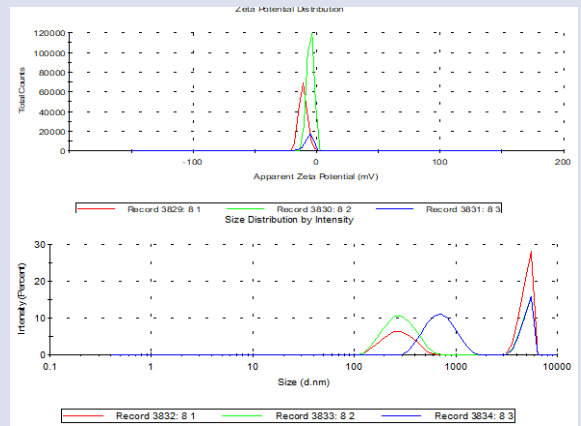
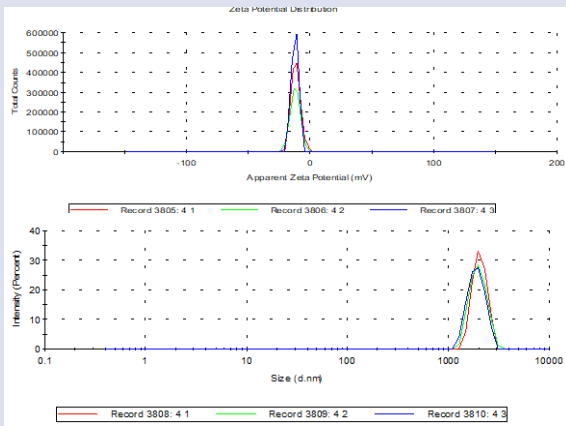
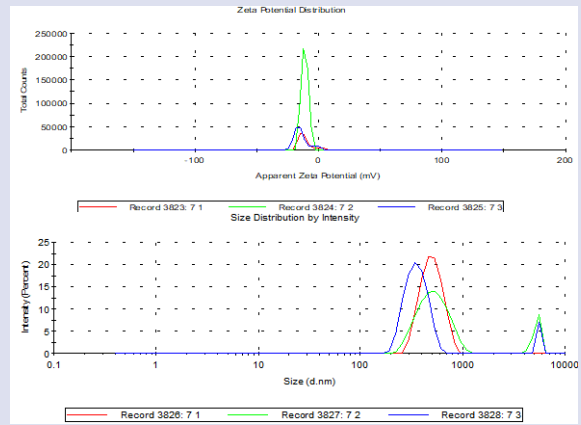
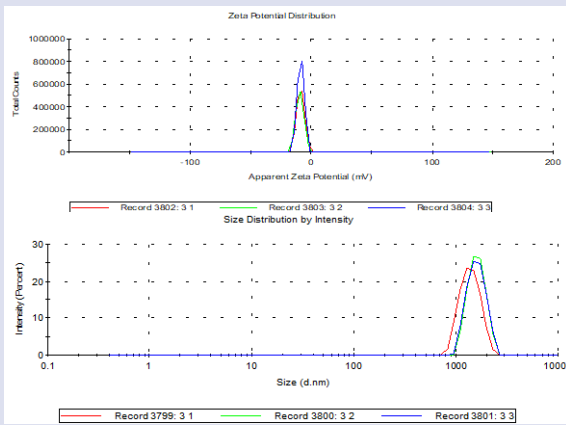
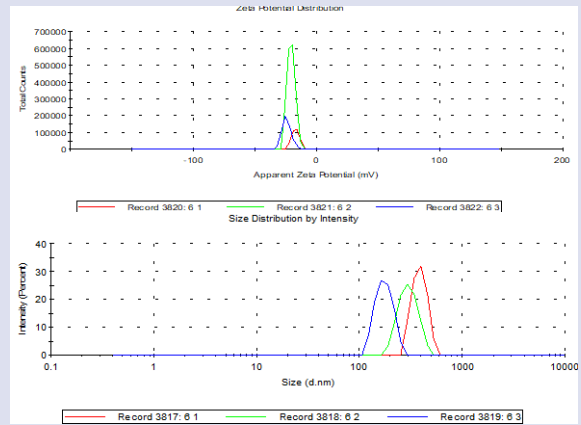
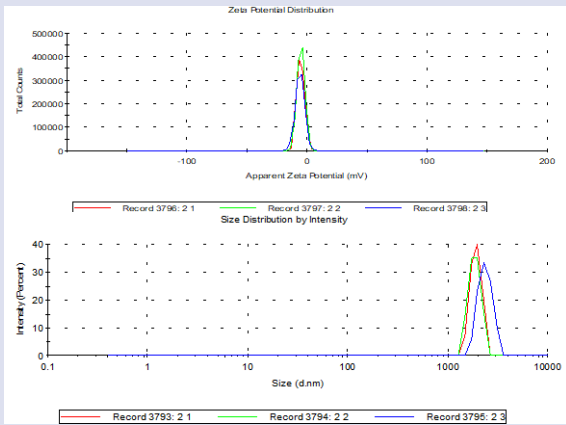
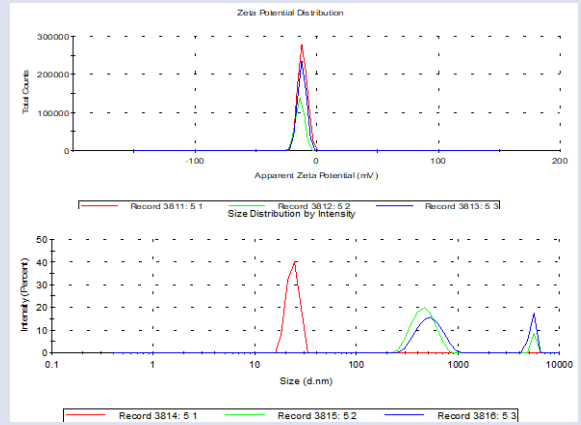
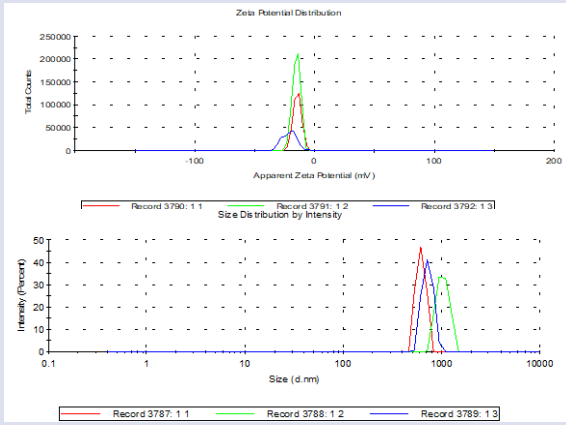


Figure 4. Zeta potential and size distribution graphs a) ZnONPs-1 b) ZnONPs-2 c) ZnONPs-3 d) ZnONPs-4 e) Fe<sub>3</sub>O<sub>4</sub>NP-1 f) Fe<sub>3</sub>O<sub>4</sub>NP-2 g) Fe<sub>3</sub>O<sub>4</sub>NP-3 h) Fe<sub>3</sub>O<sub>4</sub>NP-4

Table 3. Size distribution, PDI value, and zeta potential of ZnONPs and Fe<sub>3</sub>O<sub>4</sub>NPs synthesized from plant extracts

Samples	Z-Ave(d.nm)	Pdl	Zeta potential
ZnONPs-1	2453±285.7	0.75±0.16	-16.9±3.71
ZnONPs-2	3198±102.7	0.80±0.34	-5.35±0.49
ZnONPs-3	2204±165.9	0.30±0.10	-8.85±0.38
ZnONPs-4	2344±286.3	0.29±0,21	-11.9±0.47
Fe <sub>3</sub> O <sub>4</sub> NP-1	2537±1845	0.86±0.12	-12.5±1.18
Fe <sub>3</sub> O <sub>4</sub> NP-2	1417±286.3	0.85±0.12	-20.7±3.5
Fe <sub>3</sub> O <sub>4</sub> NP-3	1083±241.3	0.67±0.14	-12.1±1.85
Fe <sub>3</sub> O <sub>4</sub> NP-4	1341±529.	0.72±0.15	-7.43±3.1

**Antimicrobial Activity**

The antimicrobial activities of all ZnO and Fe<sub>3</sub>O<sub>4</sub>NP samples are shown in Figure 5 and Table 4.

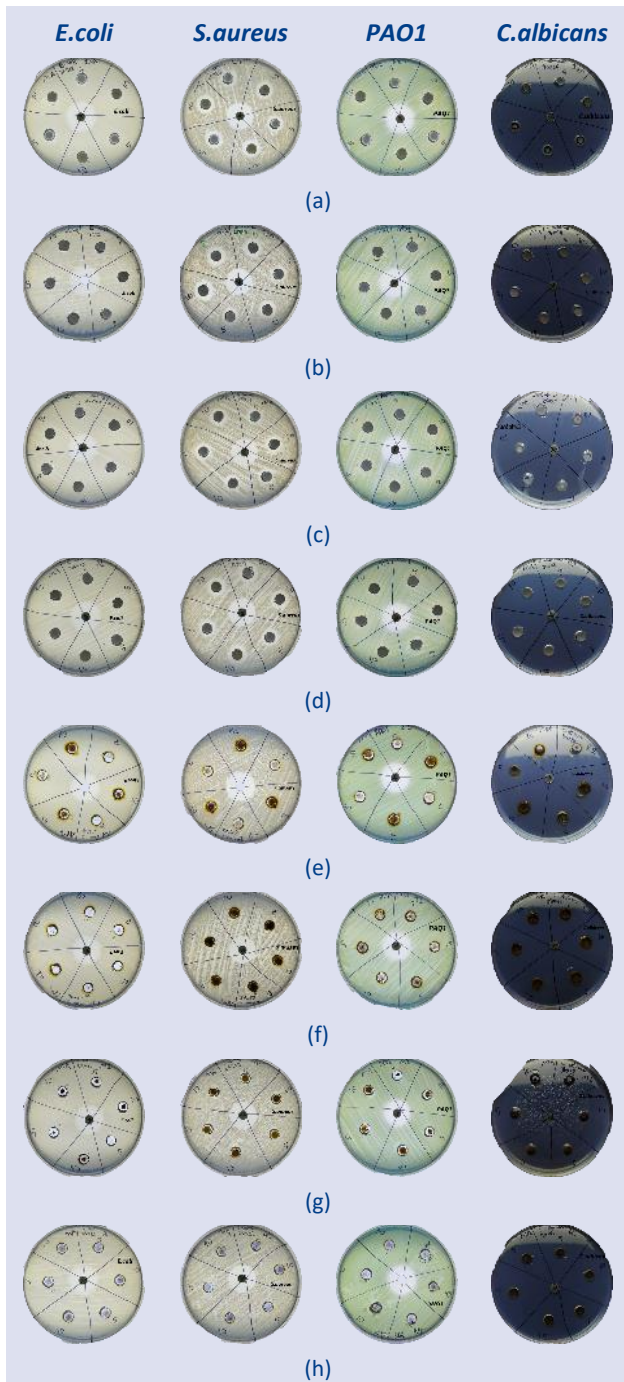


Figure 5. Antimicrobial effect of a) ZnONPs-1 b) ZnONPs-2 c) ZnONPs-3 d) ZnONPs-4 e) Fe<sub>3</sub>O<sub>4</sub>NPs-1 f) Fe<sub>3</sub>O<sub>4</sub>NPs -2 g) Fe<sub>3</sub>O<sub>4</sub>NPs -3 h) Fe<sub>3</sub>O<sub>4</sub>NPs -4

The results showed that all ZnO nanoparticles exhibited antimicrobial activity against the *S. aureus* strain alone (Figure 5). However, the Fe<sub>3</sub>O<sub>4</sub>NPs did not show any antibacterial effects against any strain. When the inhibition zone of ZnONPs was compared, no significant difference was observed in the inhibition zone of nanoparticles synthesized with different plant extracts. Furthermore, the inhibition diameters did not differ significantly at the 5 and 10 mg/mL concentrations. The size, shape, and concentration of the NPs may have been effective in preventing antimicrobial effects. Saqib et al (2018) reported that magnetic Fe<sub>3</sub>O<sub>4</sub>NPs (25-40 nm, spherical,) showed very low activity against both Gram-positive (*S. aureus*) and Gram-negative (*E. coli*) bacteria.[31].

Table 4. Inhibition zone diameter of ZnONPs and Fe<sub>3</sub>O<sub>4</sub>NP

<i>E. coli</i> 25922								
Component	ZnONPs-1	Fe <sub>3</sub> O <sub>4</sub> NPs-1	ZnONPs-2	Fe <sub>3</sub> O <sub>4</sub> NPs-2	ZnONPs-3	Fe <sub>3</sub> O <sub>4</sub> NPs-3	ZnONPs-4	Fe <sub>3</sub> O <sub>4</sub> NPs-4
5 mg/mL	-	-	-	-	-	-	-	-
10 mg/mL	-	-	-	-	-	-	-	-
Standard	18 ±0	18 ±0	18 ±0	18 ±0	18 ±0	18 ±0	18 ±0	18 ±0
<i>S. aureus</i> 25923								
Component	ZnONPs-1	Fe <sub>3</sub> O <sub>4</sub> NPs-1	ZnONPs-2	Fe <sub>3</sub> O <sub>4</sub> NPs-2	ZnONPs-3	Fe <sub>3</sub> O <sub>4</sub> NPs-3	ZnONPs-4	Fe <sub>3</sub> O <sub>4</sub> NPs-4
5 mg/mL	11 ±0	-	10 ±0	-	10 ±0	-	11 ±0	-
10 mg/mL	12 ±0	-	12 ±0	-	11 ±0	-	12 ±0	-
Standard	19 ±0	19 ±0	19 ±0	19 ±0	19 ±0	19 ±0	19 ±0	19 ±0
<i>P. aeruginosa</i> PAO1								
Component	ZnONPs-1	Fe <sub>3</sub> O <sub>4</sub> NPs-1	ZnONPs-2	Fe <sub>3</sub> O <sub>4</sub> NPs-2	ZnONPs-3	Fe <sub>3</sub> O <sub>4</sub> NPs-3	ZnONPs-4	Fe <sub>3</sub> O <sub>4</sub> NPs-4
5 mg/mL	-	-	-	-	-	-	-	-
10 mg/mL	-	-	-	-	-	-	-	-
Standard	18 ±0	18 ±0	18 ±0	18 ±0	18 ±0	18 ±0	18 ±0	18 ±0
<i>C. albicans</i> 90028								
Component	ZnONPs-1	Fe <sub>3</sub> O <sub>4</sub> NPs-1	ZnONPs-2	Fe <sub>3</sub> O <sub>4</sub> NPs-2	ZnONPs-3	Fe <sub>3</sub> O <sub>4</sub> NPs-3	ZnONPs-4	Fe <sub>3</sub> O <sub>4</sub> NPs-4
5 mg/mL	-	-	-	-	-	-	-	-
10 mg/mL	-	-	-	-	-	-	-	-
Standard	23 ±0	23 ±0	23 ±0	23 ±0	23 ±0	23 ±0	23 ±0	23 ±0



## Conclusion

In essence, nanoparticle synthesis using plant extracts offers a sustainable, biocompatible, and versatile approach with a wide range of potential applications in fields ranging from healthcare to environmental science. This approach aligns with the growing emphasis on green and sustainable nanotechnology practices while providing tailored nanomaterials for specific needs. Hence, the study involved the assessment of various plant extracts and their impacts on nanoparticle synthesis. ZnO and magnetic Fe<sub>3</sub>O<sub>4</sub> NPs were synthesised by using green synthesis method. Based on the TEM analysis results, different plant extracts had no discernible impact on nanoparticle shapes, but they did influence the size distribution. Specifically, ZnONP-1 exhibited a small crystalline size and exceptional stability. In contrast, Fe<sub>3</sub>O<sub>4</sub>NP-3 displayed a reduced crystallite size, while Fe<sub>3</sub>O<sub>4</sub>NP-2 possessed high stability according to XRD and zeta potential results. Upon examination of the antimicrobial activity results, it was found that only all ZnO nanoparticles displayed activity against the *S. aureus* strain. In conclusion, it is important to note that the choice of the plant in nanoparticle synthesis is a critical factor that can be tailored to achieve desired nanoparticle characteristics and biological activities, making it essential in designing nanoparticles for specific application.

## Conflicts of interest

The authors report no conflicts of interest in this work.

## Reference

- [1] N. Joudeh and D. Linke, Nanoparticle classification, physicochemical properties, characterization, and applications: a comprehensive review for biologists, *J Nanobiotechnology* 20 (1) (2022) 1–29.
- [2] Yusuf et al., Nanoparticles as Drug Delivery Systems: A Review of the Implication of Nanoparticles' Physicochemical Properties on Responses in Biological Systems, *Polymers (Basel)* 15 (7) (2023).
- [3] Khan, K. Saeed, and I. Khan, Nanoparticles: Properties, applications and toxicities, *Arabian Journal of Chemistry* 12 (7) (2019) 908–931.
- [4] J. Ali et al., Green synthesized zinc oxide nanostructures and their applications in dye-sensitized solar cells and photocatalysis: A review, *Mater Today Commun* 36 (August) (2023) 106840.
- [5] J.R. Vargas-Ortiz, C. Gonzalez, and K. Esquivel, Magnetic Iron Nanoparticles: Synthesis, Surface Enhancements, and Biological Challenges, *Processes* 10 (11) (2022).
- [6] H. Chopra et al., Green Metallic Nanoparticles: Biosynthesis to Applications, *Front Bioeng Biotechnol* 10 (April) (2022) 1–29.
- [7] Alayli et al., Synthesis of Nanoparticles by Green Synthesis Method, *International Journal of Innovative Research and Reviews* 1 (1) (2017) 6–9.
- [8] Chaudhary et al., Antimicrobial activity of zinc oxide nanoparticles synthesized from Aloe vera peel extract, *SN Appl Sci* 1 (1) (2019) 1–9.
- [9] M.F. Sohail et al., Green synthesis of zinc oxide nanoparticles by Neem extract as multi-facet therapeutic agents, *J Drug Deliv Sci Technol* 59 (June) (2020) 101911.
- [10] G.A. Naikoo et al., Bioinspired and green synthesis of nanoparticles from plant extracts with antiviral and antimicrobial properties: A critical review, *Journal of Saudi Chemical Society* 25 (9) (2021) 101304.
- [11] I.K. Siakavella et al., Effect of plant extracts on the characteristics of silver nanoparticles for topical application, *Pharmaceutics* 12 (12) (2020) 1–17.
- [12] P.D. Twilley, S. Rademan, and N. Lall, Are medicinal plants effective for skin cancer?, in *Medicinal Plants for Holistic Health and Well-Being*, Elsevier, (2017): pp. 13–75.
- [13] B. Feng et al., Basil polysaccharide inhibits hypoxia-induced hepatocellular carcinoma metastasis and progression through suppression of HIF-1 $\alpha$ -mediated epithelial-mesenchymal transition, *Int J Biol Macromol* 137 (2019) 32–44.
- [14] I. Rahayu, Casey Christiany, and Susana Elya Sudrajat, The Potency of Cinnamomum Zeylanicum to Prevent Diseases: a Review, *Eureka Herba Indonesia* 2 (1) (2021) 52–62.
- [15] Z. Wang et al., Origins, phytochemistry, pharmacology, analytical methods and safety of cortex moutan (*paenonia suffruticosa* Andrew): A systematic review, *Molecules* 22 (6) (2017).
- [16] A. Ozdemir, Antioxidant Capacity And Antimicrobial Activity of *Paeonia Peregrina* L [Usak-Itecik Tulip] Extracts and Its Phenolic and Flavonoid Compounds, *The Ulutas Medical Journal* 5 (4) (2019) 1.
- [17] G. Athanasakis et al., Antioxidant properties of the wild edible mushroom *Lactarius salmonicolor*, *J Med Food* 16 (8) (2013) 760–764.
- [18] B.O. Asimeng et al., Characterization and Inhibitory Effects of Magnetic Iron Oxide Nanoparticles Synthesized from Plant Extracts on HeLa Cells, *Int J Biomater* 2020 (2020) 15–18.
- [19] P. Sharma et al., Application of ZnO-based nanocomposites for vaccines and cancer immunotherapy, *Pharmaceutics* 11 (10) (2019) 6–10.
- [20] A. Naveed Ul Haq et al., Synthesis Approaches of Zinc Oxide Nanoparticles: The Dilemma of Ecotoxicity, *J Nanomater* 2017 (Table 1) (2017).
- [21] G.T. Mazitova et al., Synthesis and Properties of Zinc Oxide Nanoparticles: Advances and Prospects, *Rev J Chem* 9 (2) (2019) 127–152.
- [22] K. Parajuli, A.K. Sah, and H. Paudyal, Green Synthesis of Magnetite Nanoparticles Using Aqueous Leaves Extracts of *Azadirachta indica*; and Its Application for the Removal of As(V) from Water, *Green and Sustainable Chemistry* 10 (04) (2020) 117–132.
- [23] K. Handore et al., Novel green route of synthesis of ZnO nanoparticles by using natural biodegradable polymer and its application as a catalyst for oxidation of aldehydes, *Journal of Macromolecular Science, Part A: Pure and Applied Chemistry* 51 (12) (2014) 941–947.
- [24] R. Gomathi, H. Suhana, and D. Paradesi, Characterization Study of Cytotoxicity of Green Synthesized ZnO Nanoparticles Loaded with Anti-Cancer Doxorubicin Drug, *ChemistrySelect* 6 (18) (2021) 4533–4538.
- [25] M.B. Nayan et al., Comparative Study on the Effects of Surface Area, Conduction Band and Valence Band Positions on the Photocatalytic Activity of ZnO-M<sub>x</sub>O<sub>y</sub>-Heterostructures, *J Water Resour Prot* 11 (03) (2019) 357–370.



- [26] F. Ahangaran, A. Hassanzadeh, and S. Nouri, Surface modification of Fe<sub>3</sub>O<sub>4</sub>@SiO<sub>2</sub> microsphere by silane coupling agent, *Int Nano Lett* 3 (1) (2013).
- [27] C.M. Hoo et al., A comparison of atomic force microscopy (AFM) and dynamic light scattering (DLS) methods to characterize nanoparticle size distributions, *Journal of Nanoparticle Research* 10 (SUPPL. 1) (2008) 89–96.
- [28] M. Danaei et al., Impact of particle size and polydispersity index on the clinical applications of lipidic nanocarrier systems, *Pharmaceutics* 10 (2) (2018) 1–17.
- [29] R. Xu, Progress in nanoparticles characterization: Sizing and zeta potential measurement, *Particuology* 6 (2) (2008) 112–115.
- [30] S.C. Endres, L.C. Ciacchi, and L. Mädler, A review of contact force models between nanoparticles in agglomerates, aggregates, and films, *J Aerosol Sci* 153 (November 2020) (2021).
- [31] S. Saqib et al., Synthesis, characterization and use of iron oxide nano particles for antibacterial activity, *Microsc Res Tech* 82 (4) (2019) 415–420.